

Dynamical Quantum Phase Transitions in Boundary Time Crystals

Sukrut Mondkar,* Priya Ghosh,† and Ujjwal Sen‡
*Harish-Chandra Research Institute, A CI of Homi Bhabha National Institute,
 Chhatnag Road, Jhusi, Prayagraj (Allahabad) 211019, India*

We demonstrate the existence of a dynamical quantum phase transition (DQPT) in a dissipative collective-spin model that exhibits the boundary time crystal (BTC) phase. We initialize the system in the ground state of the Hamiltonian in either the BTC or the non-BTC phase, and drive it across the BTC transition. The driving is done by an abrupt quench or by a finite-time linear ramp of a Hamiltonian control parameter under Markovian Lindblad dynamics. We diagnose DQPTs through zeros of the fidelity-based Loschmidt echo between the initial state and the evolving mixed state, which induce nonanalytic cusp-like features in the associated rate function. For quenches into the BTC phase, the Loschmidt echo exhibits repeated zeros due to the emergent time-periodic steady state, whereas for quenches into the non-BTC phase, the overlap vanishes and remains zero once the dynamics relaxes to a stationary state. We further show that the DQPT persists under the ramp protocol followed by unitary evolution with the final Hamiltonian. Finally, we analyze the finite-size scaling of the first critical time and find convergence to a constant in the thermodynamic limit, with distinct power-law approaches for the quench and the ramp protocols.

I. INTRODUCTION

Time crystals are non-equilibrium phases of matter in which time-translation symmetry is spontaneously broken. The original proposal of a time crystal in thermal equilibrium by Wilczek [1] was ruled out by no-go theorems [2–4], establishing that spontaneous breaking of continuous time-translation symmetry cannot occur in thermal equilibrium. Nevertheless, the time-crystal phase can be realized away from equilibrium in both periodically driven closed and open many-body quantum systems [5–9]. Time crystals are broadly classified into two categories, viz., discrete time crystals (DTC) and continuous time crystals (CTC) based on whether a discrete or a continuous time translation symmetry is spontaneously broken in the time crystal phase. In the widely studied setting of DTC, a periodically driven (Floquet) system spontaneously breaks the discrete time-translation symmetry of the drive Hamiltonian, typically via mechanisms such as many-body localization [9–14] or prethermalization [15–19].

In a conceptually distinct route to time-crystalline order, the so-called boundary time crystals (BTCs) arise in time-independent open quantum many-body systems with time-independent dynamical generator in which persistent oscillations appear in the long-time steady-state dynamics without any external periodic drive. This phenomenon was first identified in Ref. [20], where the interplay of Hamiltonian interactions and collective dissipation generates a time-periodic steady state despite the fact that the Hamiltonian is time independent. Necessary conditions responsible for the emergence of BTCs have been identified in Refs. [21, 22], and a growing

body of work has explored various aspects of BTCs and their applications [23–40]. In particular, BTCs have been shown to provide advantages for quantum metrology and sensing [28, 30, 31, 35, 38, 40] and have also been investigated from a quantum-thermodynamic perspective [29, 32].

In parallel, another major development in nonequilibrium quantum many-body physics is the notion of a dynamical quantum phase transition (DQPT) [41, 42]. Quantum phase transitions [43, 44] are a central paradigm in the theory of quantum many-body systems at equilibrium. They occur at zero temperature and are driven by quantum fluctuations, manifesting as nonanalytic behavior of ground-state properties when a Hamiltonian control parameter is tuned across a critical value in the thermodynamic limit. While equilibrium quantum phase transitions are by now well understood, much less is known about their dynamical counterparts that arise during nonequilibrium time evolution. These DQPTs are characterized by nonanalytic structures emerging in real time during unitary or dissipative evolution following a quench or ramp of system parameters. In the standard closed-system quench protocol, the system is initialized in the ground state of an initial Hamiltonian, following which the Hamiltonian is subjected to a sudden change in one of its parameters. Subsequently, the system evolves with the time-independent post-quench Hamiltonian. The return probability to the initial state, quantified by the Loschmidt echo, can develop zeros at critical times, signaling the onset of DQPT. Correspondingly, the associated rate function (often interpreted as a dynamical free-energy density) develops cusp-like nonanalyticities at those critical times in the thermodynamic limit. DQPTs have been observed experimentally in a variety of platforms [45–55]. For reviews on DQPT, see Refs. [42, 56, 57]. Importantly for the present work, DQPTs also occur in open quantum systems, where the Loschmidt echo can be generalized using fidelity between mixed states [58].

* sukrutmondkar@gmail.com

† priyaghosh1155@gmail.com

‡ uijwal@hri.res.in

These developments motivate a natural question: how do DQPTs manifest in intrinsically non-equilibrium time-crystalline phases that are stabilized by dissipation? While DQPTs have been explored in a broad range of dissipative models [58–68], their interplay with the BTC phase, where the late-time state is time-periodic rather than stationary, has not been explored. In this context, it has been shown that discrete time crystals in closed quantum systems can host DQPTs [69]. In this work, we demonstrate the existence of DQPTs in a dissipative collective-spin model that exhibits the BTC phase under Markovian Lindblad dynamics. We initialize the system in the ground state of the Hamiltonian in one phase (BTC or non-BTC), and then drive the system across the BTC transition using either (i) an abrupt quench or (ii) a finite-time linear ramp of a Hamiltonian control parameter. We diagnose DQPTs using zeros of the fidelity-based Loschmidt echo between the initial state and the time-evolved mixed state, which induce cusp-like nonanalyticities in the corresponding rate function.

Our results reveal a qualitative distinction tied to the nature of the late-time dynamics. For quenches into the BTC phase, the time-periodic steady state leads to repeated zeros of the fidelity-based Loschmidt echo at a sequence of critical times. In contrast, for quenches into the non-BTC phase, the dynamics relaxes to a stationary steady state, and the overlap with the pre-quench initial state can vanish and remain zero beyond the first critical time. We further show that the DQPT persists under ramp protocols followed by unitary evolution with the final Hamiltonian. Finally, in both the quench and ramp protocols, we analyze finite-size scaling of the first critical time and find convergence to a constant in the thermodynamic limit, with distinct power-law approaches for quench and ramp protocols.

The remainder of the paper is organized as follows. In Sec. II we briefly review BTCs and DQPTs, including the fidelity-based Loschmidt echo appropriate for diagnosing DQPTs in open-system dynamics. In Sec. III, we describe the collective-spin model and the quench and the ramp protocols used to probe DQPTs across the BTC transition. In Sec. IV we present our numerical results and finite-size scaling analysis. We conclude in Sec. V.

II. PRELIMINARIES

A. Boundary Time Crystals

The boundary time crystal (BTC) is an intrinsically non-equilibrium phase of open many-body systems in which the long-time dynamics exhibits persistent oscillations despite a time-independent generator of evolution. Concretely, in the BTC phase, the system relaxes to a time-periodic steady state, so that expectation values of suitable observables display stable oscillations at late times. In a Markovian description, this behavior is naturally characterized via the spectrum of the Liou-

villian superoperator. The emergence of undamped oscillations is associated with purely imaginary Liouvillian eigenvalues, leading to time-translation-symmetry breaking in the steady-state dynamics. The BTC phase was first identified in Ref. [20] in the context of collective spin models originally introduced to describe cooperative emission of radiation in cavity-QED type settings [70–73].

The BTC phase can be diagnosed operationally by (i) persistent oscillations of collective observables (e.g. average magnetization) at late times, and (ii) the corresponding Liouvillian spectral signature mentioned above. As a representative example, we consider the collective-spin model of Ref. [23] comprising N spin-1/2 particles, whose Hamiltonian and Lindblad operator take the form,

$$H = K \left(\omega_0 S^x + \frac{\omega_x}{S} (S^x)^2 + \frac{\omega_z}{S} (S^z)^2 \right), \quad (1)$$

$$L = \sqrt{\frac{K\kappa}{S}} S_- \quad (2)$$

where $S = N/2$ is the total spin of the system, $S^\alpha = \sum_{j=1}^N \sigma_j^\alpha / 2$ with $\alpha = x, y, z$ are collective spin operators, $S_\pm = S^x \pm iS^y$ and σ_j^α are the Pauli spin operators for the j th spin. Note that K is a constant parameter with units of energy. In this paper, we express all the physical quantities in units of $K = 1$. All the parameters ω_0 , ω_x , ω_z , and κ are dimensionless. For appropriate parameter regimes, this model exhibits a BTC phase in which the long-time dynamics displays robust oscillations of collective observables, whereas outside that regime the system relaxes to a stationary time-independent steady state [23]. In what follows, we refer to these regimes as the BTC and non-BTC phases, respectively.

B. Dynamical Quantum Phase Transitions

Dynamical quantum phase transitions (DQPTs) [41, 42] are characterized by the non-analyticities in the real-time evolution of a quantum many-body system, induced by a time-independent final Hamiltonian after either an abrupt quench or a gradual change in a Hamiltonian parameter. Consider a quantum many-body system of size N described by a Hamiltonian H , initially prepared in the ground state of H , $|\psi(0)\rangle$ at time $t = 0$. Note that t denotes dimensionless time which is related to the actual time \tilde{t} by $t = \frac{K\tilde{t}}{\hbar}$. At this instant, a control parameter λ in the Hamiltonian is abruptly quenched from an initial value λ_i to a final value λ_f . The subsequent dynamics is governed by the time-independent Hamiltonian $H(\lambda_f)$, such that the state at time t evolves as $|\psi(t)\rangle = \exp(-iH(\lambda_f)t) |\psi(0)\rangle$. A DQPT is said to occur at critical times for which the evolved state becomes orthogonal to the initial state. Equivalently, these critical times are marked by the vanishing of the Loschmidt echo (LE), $\mathcal{L} := |\langle\psi(0)|\psi(t)\rangle|^2$. At those times, the associated dynamical free-energy density, or the rate function of the return probability, $f := -\lim_{N \rightarrow \infty} (1/N) \ln \mathcal{L}$, diverges.

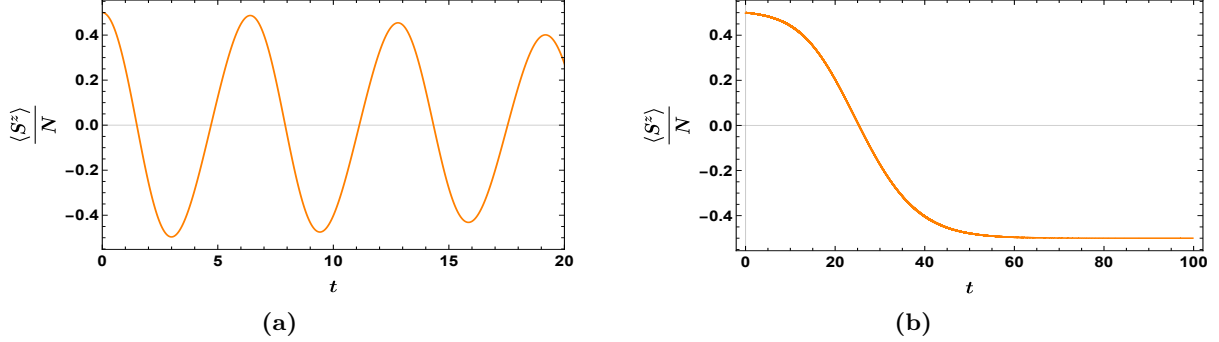


FIG. 1. *Illustration of BTC and non-BTC phases in the model of Eq. (7).* Shown is the average magnetization $\langle S^z \rangle/N$ for $N = 100$ as a function of time in (a) the BTC phase and (b) the non-BTC phase. In the BTC regime, the dynamics of the order parameter $\langle S^z \rangle/N$ relaxes to a time-periodic steady state with persistent oscillations, whereas in the non-BTC regime, the average magnetization approaches a time-independent stationary value. The parameters corresponding to the BTC phase are chosen as $\omega_0 = -1$, $\omega_x = 0$, $\omega_z = -0.25$, and $\kappa = 0.1$. For the non-BTC phase, we set $\omega_0 = 0$, while keeping all other parameters unchanged. The quantities plotted along the horizontal and vertical axes in each panel are dimensionless.

Such non-analyticities also appear when the Hamiltonian control parameter is changed via a slow ramping protocol instead of sudden quenching [76, 77].

DQPTs have also been shown to exist under dissipative dynamics [58–68]. For open-system dynamics, the Loschmidt echo is naturally generalized using the Uhlmann fidelity [78, 79]. For two density matrices ρ and σ , the Uhlmann fidelity is

$$F(\rho, \sigma) := \left[\text{Tr} \sqrt{\sqrt{\rho} \sigma \sqrt{\rho}} \right]^2. \quad (3)$$

We define the fidelity-based Loschmidt echo (FLE) as

$$\mathcal{L}_F(t) := F(\rho(0), \rho(t)), \quad (4)$$

and the corresponding rate function as

$$f_F(t) := - \lim_{N \rightarrow \infty} \frac{1}{N} \ln \mathcal{L}_F(t). \quad (5)$$

DQPT critical times are then identified by zeros of $\mathcal{L}_F(t)$, at which $f_F(t)$ develops cusp-like singularities. In the special case where the initial state is pure, $\rho(0) = |\psi(0)\rangle\langle\psi(0)|$, Eq. (4) reduces to

$$\mathcal{L}_F(t) = \langle\psi(0)|\rho(t)|\psi(0)\rangle. \quad (6)$$

In this work, we use $\mathcal{L}_F(t)$ and $f_F(t)$ as diagnostics of DQPTs under Lindblad evolution, and we consider both abrupt quenches and finite-time ramp protocols across the BTC transition.

III. SETUP

We consider a system of N spin-1/2 particles described by a collective-spin Hamiltonian H of Eq. (1) which evolves under Markovian dynamics with a single jump

operator L given in Eq. (2). The Markovian dynamics is governed by the Lindblad master equation,

$$\begin{aligned} \frac{d\rho}{dt} &= \mathcal{L}[\rho] = -i[H, \rho] + \mathcal{D}[\rho], \\ \mathcal{D}[\rho] &= L\rho L^\dagger - \frac{1}{2}\{L^\dagger L, \rho\}. \end{aligned} \quad (7)$$

This model supports both a BTC regime, in which the long-time steady state is time periodic, and a non-BTC regime, in which the dynamics relaxes to a stationary steady state [23]. In the BTC phase, the average magnetization, $\langle S^z \rangle/N$, varies periodically in time, and the spectrum of the Liouvillian \mathcal{L} contains purely imaginary eigenvalues. In the BTC phase, such time-periodic behavior of $\langle S^z \rangle/N$ exists for all the initial states and is robust against perturbations in Hamiltonian parameters and noise [23].

To probe DQPTs across the BTC transition, we consider two standard driving protocols. In both, the system is initialized in the ground state $\rho(0) = |\psi(0)\rangle\langle\psi(0)|$ of the Hamiltonian $H(\lambda_i)$. We then vary a single Hamiltonian parameter $\lambda \in \{\omega_0, \omega_x, \omega_z\}$ either abruptly (quench protocol) or slowly (ramp protocol) from an initial value λ_i to a final value λ_f , while keeping the remaining parameters fixed. This change in Hamiltonian parameter results in the time evolution of the initial state according to the master equation (7) with the final Hamiltonian $H(\lambda_f)$. A DQPT is diagnosed by zeros of the fidelity-based Loschmidt echo $\mathcal{L}_F(t)$ introduced in Sec. II B, and also equivalently by cusp-like nonanalyticities in the corresponding rate function $f_F(t)$. Note that the change in parameter λ must be across the BTC phase transition point. In other words, if the initial Hamiltonian parameter choice corresponds to the non-BTC phase, then the final Hamiltonian parameters after quench/ramp should correspond to the BTC phase, and vice versa.

In our work (Sec. IV), we take $\lambda = \omega_0$ for concreteness; however, the protocols described below apply to varying any of the Hamiltonian parameters.

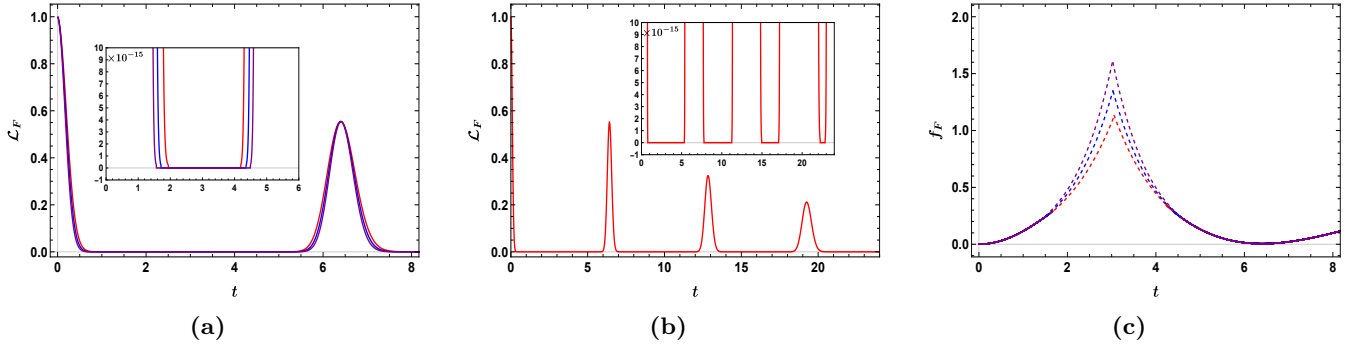


FIG. 2. *Dynamical quantum phase transition under a quench from the non-BTC to the BTC phase.* (a) The fidelity-based Loschmidt echo $\mathcal{L}_F(t)$ is shown as a function of time following an abrupt quench of ω_0 from $\omega_{0,i} = 0$ (non-BTC) to $\omega_{0,f} = -1$ (BTC) for system sizes $N = 50$ (red), $N = 60$ (blue), and $N = 70$ (purple). The system is initially prepared in the ground state of the pre-quench Hamiltonian and subsequently evolves under the Lindblad dynamics with the post-quench Hamiltonian. The first vanishing of $\mathcal{L}_F(t)$ defines the first critical time $t_c^{(1)}$, signalling the onset of a DQPT. The inset magnifies the region near the t -axis to highlight the numerical zeros. The numbers smaller than machine precision (10^{-15}) are concurrent with zero. We obtain $t_c^{(1)}$ as the midpoint of the first times at which \mathcal{L}_F drops below and rises above 10^{-15} , denoted respectively as $t_{\downarrow}^{(1)}$ and $t_{\uparrow}^{(1)}$. The values of the first critical times, $t_c^{(1)}$, along with the respective values of $t_{\downarrow}^{(1)}$ and $t_{\uparrow}^{(1)}$ for each of the three N are provided in Tab. I. The data is generated with the time-step of $\Delta t = 0.001$. (b) Plot of $\mathcal{L}_F(t)$ for $N = 250$ with same parameters as in (a) demonstrating that $\mathcal{L}_F(t)$ periodically becomes zero. (c) The rate function $f_F(t) = -(1/N) \ln \mathcal{L}_F(t)$ corresponding to (a) is shown with the curves of the same colors for the respective N values as in (a). At the first critical time $t_c^{(1)}$, where \mathcal{L}_F vanishes, f_F exhibits a cusp-like singularity, signalling a DQPT. Solid curves show numerically accessible values of f_F , while dashed curves are extrapolations inside the region where \mathcal{L}_F falls below machine precision.

A. Quench Protocol

In the quench protocol [41, 58], after preparing the initial ground state $|\psi(0)\rangle$ of $H(\lambda_i)$, we abruptly change $\lambda_i \rightarrow \lambda_f$ at $t = 0$. The state then evolves under Eq. (7) with the time-independent post-quench Hamiltonian $H(\lambda_f)$. We compute $\mathcal{L}_F(t) = F(\rho(0), \rho(t))$ whose first zero defines the first critical time and signals the onset of a DQPT.

B. Ramp Protocol

We also consider a finite-time ramp protocol introduced in Ref. [58] for detecting DQPT in open quantum systems. In the ramp protocol [58, 77], instead of abrupt quenching, the parameter λ is varied smoothly from λ_i to λ_f over a duration τ as

$$\lambda(t) = \lambda_i + (\lambda_f - \lambda_i) \frac{t}{\tau}, \quad 0 \leq t \leq \tau \quad (8)$$

During the ramp ($0 \leq t \leq \tau$), the system evolves according to Eq. (7) with a time-dependent Hamiltonian $H(\lambda(t))$. At the end of the ramp, $t = \tau$, the dissipation is switched off, and subsequently the state evolves unitarily with the final Hamiltonian $H(\lambda_f)$. Treating $\rho(\tau)$ as the initial state for this post-ramp unitary stage, we compute

$$\mathcal{L}_F(t') = F(\rho(\tau), \rho(\tau + t')), \quad t' \geq 0 \quad (9)$$

and identify DQPT critical times by zeros of $\mathcal{L}_F(t')$ (equivalently cusps in $f_F(t')$).

IV. DQPT ACROSS THE BTC TRANSITION

In this section, we demonstrate the emergence of DQPTs in the dissipative collective-spin model of Eq. (7) when a Hamiltonian control parameter is driven across the BTC/non-BTC phase boundary. We diagnose DQPTs using the fidelity-based Loschmidt echo $\mathcal{L}_F(t)$ and its rate function $f_F(t)$ introduced in Sec. II B. Critical times correspond to zeros of $\mathcal{L}_F(t)$, at which $f_F(t)$ develops nonanalytic cusp-like singularities in the thermodynamic limit.

Throughout this section we vary $\lambda = \omega_0$ while keeping $\omega_x = 0$, $\omega_z = -0.25$, and $\kappa = 0.1$ fixed. For the non-BTC \rightarrow BTC protocols we choose $\omega_{0,i} = 0$ (non-BTC) and $\omega_{0,f} = -1$ (BTC), while for the BTC \rightarrow non-BTC ones we choose $\omega_{0,i} = -1$ (BTC) and $\omega_{0,f} = 0$ (non-BTC). The corresponding long-time behavior of the order-parameter observable, namely, average magnetization $\langle S^z \rangle / N$ is shown in Fig. 1 for $N = 100$. In the BTC regime, the magnetization exhibits persistent oscillations in time, whereas in the non-BTC regime, it relaxes to a time-independent stationary value.

Numerical convention for identifying zeros. In finite-precision numerics, $\mathcal{L}_F(t)$ does not typically hit exact zero. We therefore treat values below a threshold ε as numerically zero, and define the first critical time $t_c^{(1)}$ as the midpoint

$$t_c^{(1)} = \frac{t_{\uparrow}^{(1)} + t_{\downarrow}^{(1)}}{2} \quad (10)$$

N	$t_{\downarrow}^{(1)}$	$t_{\uparrow}^{(1)}$	$t_c^{(1)}$
50	1.869	4.232	3.051
60	1.666	4.398	3.032
70	1.522	4.530	3.026

TABLE I. *Quench protocol: non-BTC \rightarrow BTC*. The values of $t_{\downarrow}^{(1)}$, $t_{\uparrow}^{(1)}$, and $t_c^{(1)}$ in Fig. 2 (a) corresponding to $N = 50, 60$, and 70 .

where $t_{\uparrow}^{(1)}$ ($t_{\downarrow}^{(1)}$) is the first time at which $\mathcal{L}_F(t)$ drops below (rises above) ε . For quenches, we can take $\varepsilon = 10^{-15}$ (machine precision), while for the ramp protocol, we use $\varepsilon = 10^{-13}$ due to enhanced numerical noise in mixed-state fidelity evaluations for large N . We use a time step $\Delta t = 0.001$ throughout.

A. Quench Protocol

Let us first discuss the quench protocol from the stationary non-BTC regime to the BTC regime. Fig. 2 (a) displays a plot of $\mathcal{L}_F(t) = F(\rho(0), \rho(t))$ as a function of time for $N = 50$ (red), $N = 60$ (blue), and $N = 70$ (purple). The first interval where $\mathcal{L}_F(t)$ falls below 10^{-15} defines $t_{\downarrow}^{(1)}$ and $t_{\uparrow}^{(1)}$, and the resulting $t_c^{(1)}$ values are reported in Tab. I.

Since the initial state is the pure ground state $\rho(0) = |\psi(0)\rangle\langle\psi(0)|$ of $H(\omega_{0,i})$, the fidelity-based Loschmidt echo simplifies to the overlap

$$\mathcal{L}_F(t) = \langle\psi(0)|\rho(t)|\psi(0)\rangle \quad (11)$$

The corresponding rate function $f_F(t)$ is plotted in Fig. 2 (c). At the first critical time $t_c^{(1)}$, the echo vanishes (within numerical precision), and $f_F(t)$ diverges accordingly. Within the accessible numerical precision, we are able to numerically compute f_F for the values of t for which $\mathcal{L}_F > 10^{-15}$ (machine precision). Since for the values of t for which $\mathcal{L}_F \leq 10^{-15}$, we set \mathcal{L}_F to zero, the value of f_F for all these times is divergent within the numerical precision. The solid curves in Fig. 2 (c) depict f_F for the times where $\mathcal{L}_F > 10^{-15}$. We extrapolate this f_F to the region where $\mathcal{L}_F \leq 10^{-15}$ and represent these extrapolated curves by dashed lines of respective colors. This extrapolation is done by fitting the curve to the left of $t_c^{(1)}$ by an exponential function of the form, $a_L e^{b_L(t-t_c^{(1)})} + c_L$ where a_L , b_L , and c_L are fitting parameters, and fitting the curve to the right of $t_c^{(1)}$ by another exponential function of the form $a_R e^{b_R(t_c^{(1)}-t)} + c_R$, where a_R , b_R , and c_R being the corresponding fitting parameters. The two extrapolated curves meet at $t = t_c^{(1)}$, culminating in a visible cusp. Note that this extrapolation to display the cusp is solely for the representative purpose.

A qualitative feature specific to quenches into the BTC phase is that zeros of $\mathcal{L}_F(t)$ also occur at times later than $t_c^{(1)}$. Because the long-time dynamics approach a

time-periodic steady state in the BTC regime, the evolving state can repeatedly become orthogonal to the initial state at a sequence of critical times, while returning to nonzero overlap at intermediate times. This behavior is visible in Fig. 2 (b) which depicts the plot of $\mathcal{L}_F(t)$ for $N = 250$ with the same parameter values as in Fig. 2 (a).

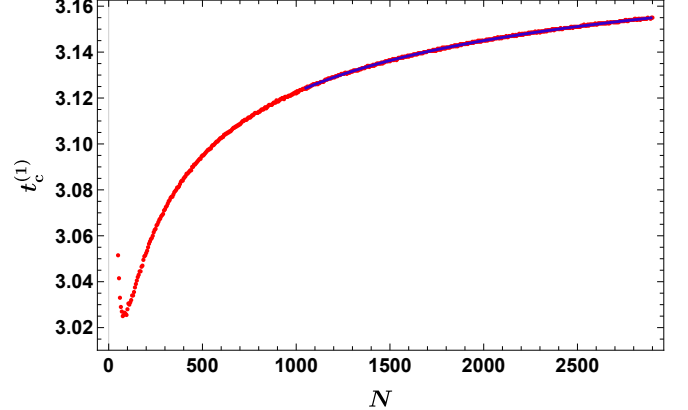


FIG. 3. *Finite-size scaling of the first critical time under a quench from the non-BTC to the BTC phase*. The first critical time $t_c^{(1)}$ is plotted as a function of system size N . The red dots are the numerical data, while the blue curve is a power-law fit of the form $t_c^{(1)}(N) = aN^{-b} + c$ in the range $N \in [1045, 2900]$, indicating convergence to a constant value in the thermodynamic limit. The best-fit values of fitting parameters are $a = -1.194 \pm 0.053$, $b = 0.354 \pm 0.009$, and $c = 3.225 \pm 0.002$. Since the data is generated with a time resolution of $\Delta t = 0.001$, values of the parameters up to the third decimal place are meaningful. Therefore, we have truncated the errors to the third decimal place. The RMS fitting error is less than 0.001. The values of both pre- and post-quench parameters are the same as in Fig. 2.

Furthermore, we have investigated the scaling of $t_c^{(1)}$ with the system size N and found the asymptotic value of $t_c^{(1)}$ in the thermodynamic limit, $N \rightarrow \infty$. The plot of $t_c^{(1)}$ as a function of N is shown in Fig. 3 for the same values of parameters used in Fig. 2. The red dots constitute the actual data generated for $N = 50$ to $N = 2900$ in steps of 5. We observe that $t_c^{(1)}$ initially decreases, followed by a subsequent increase, and it approaches a constant value asymptotically for large N . The blue curve is the best power-law fit of the form $t_c^{(1)}(N) = aN^{-b} + c$ in the range $1045 < N < 2900$ for the $t_c^{(1)}(N)$ data used to generate the red curve. The best-fit values of parameters are $a = -1.194 \pm 0.053$, $b = 0.354 \pm 0.009$, and $c = 3.225 \pm 0.002$. Since the data is generated with a time resolution of $\Delta t = 0.001$, values of the parameters up to the third decimal place are meaningful. Therefore, we have truncated the best-fit parameter values and their errors to the third decimal place. The root-mean-square (RMS) fitting error is zero up to the third decimal place. In other words, we find that in the $N \rightarrow \infty$ limit $t_c^{(1)}$ approaches a constant value of 3.225 via a power-law with

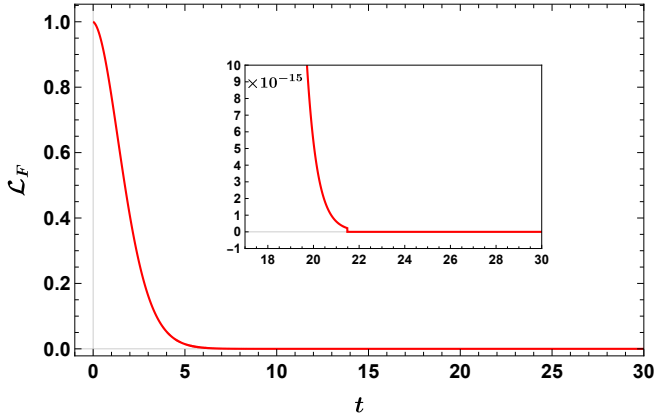


FIG. 4. *DQPT under a quench from the BTC to the non-BTC phase.* The fidelity-based Loschmidt echo $\mathcal{L}_F(t)$ is shown for $N = 100$ following a quench of ω_0 from $\omega_{0,i} = -1$ (BTC) to $\omega_{0,f} = 0$ (non-BTC). After the first vanishing of \mathcal{L}_F at $t_c^{(1)} = 20.778$, the overlap remains zero as the dynamics relaxes to a stationary steady state. The inset highlights the behavior near the t -axis. Unlike quenches into the BTC phase, no revivals of the overlap occur at later times.

Fitting function	Fitted parameters	RMS error
$aN^{-b} + c$	$a = -1.194 \pm 0.053$	$< 10^{-3}$
	$b = 0.354 \pm 0.009$	
	$c = 3.225 \pm 0.002$	
$a \exp(-N^b) + c$	$a = -1.505 \pm 0.025$	$< 10^{-3}$
	$b = 0.157 \pm 0.001$	
	$c = 3.199 \pm 0.001$	
$a \ln(N) + c$	$a = 0.029 \pm (< 10^{-3})$	$< 10^{-3}$
	$c = 2.918 \pm (< 10^{-3})$	

TABLE II. *Finite-size scaling of $t_c^{(1)}$ for quench protocol from non-BTC to BTC.* The fitting functions and corresponding best-fit values of fitting parameters, along with their errors, are shown. The last column shows the overall root-mean-square (RMS) fitting error. The data used for fitting is the data indicated by red dots in Fig. (3) within the range $1045 < N < 2900$. We have truncated all the numerical values to the third decimal place as the time resolution of our numerics is $\Delta t = 0.001$.

an exponent of 0.354.

We have also fitted the same data of Fig. 3 with exponential and log functions. The corresponding values of fitted parameters and errors are reported in Tab. II. Observation that the exponential fit performs comparable to the power-law fit can be explained as follows. First note that $N^{-0.354}$ can be written as $e^{-0.354 \ln N}$, whereas the exponential function goes as $e^{-N^{0.157}}$. Both $N^{0.157}$ and 0.354 ln N are close to each other for the range $1045 < N < 2900$ used for the fitting. This is why the performance of both the power-law and exponential fits is comparable. However, it can be easily seen that the function $N^{0.157}$ significantly dominates over $0.354 \ln N$ for $N > 10^9$ and therefore in the thermodynamic limit $N \rightarrow \infty$, the two functions will have completely disparate

asymptotic behaviors.

Finally, we also confirm that a DQPT occurs for quenches in the opposite direction, BTC \rightarrow non-BTC. Fig. 4 shows $\mathcal{L}_F(t)$ for $N = 100$ when quenching from $\omega_{0,i} = -1$ to $\omega_{0,f} = 0$. Here $\mathcal{L}_F(t)$ drops below numerical precision at $t_c^{(1)} = 20.778$ and remains zero thereafter. Since when the post-quench Hamiltonian corresponds to non-BTC phase, the state of the system reaches a time-independent stationary state, vanishing of \mathcal{L}_F for this late time stationary state with respect to the pre-quench initial state implies that the late-time stationary state becomes orthogonal to the initial state. Unlike the BTC case, here there is no late-time periodicity that could revive the overlap.

B. Ramp Protocol

We now consider the finite-time ramp protocol described in Sec. III B, where $\omega_0(t)$ is varied linearly from $\omega_{0,i} = 0$ to $\omega_{0,f} = -1$ over a duration $\tau = 5$ as

$$\omega_0(t) = \omega_{0,i} + (\omega_{0,f} - \omega_{0,i}) \frac{t}{\tau}, \quad (12)$$

with dissipation present during the ramp and switched off afterwards. We then compute $\mathcal{L}_F(t')$ during the subsequent unitary evolution using $\rho(\tau)$ (end-of-ramp state) as the reference state. Specifically,

$$\mathcal{L}_F(t') = F(\rho(\tau), \rho(\tau + t')), \quad t' \geq 0$$

as defined before in Eq. (9).

Fig. 5 (a) shows the plot of \mathcal{L}_F for the ramp protocol with $N = 70$ (red), $N = 80$ (blue), and $N = 90$ (purple). In contrast to the quench protocol, the reference state $\rho(\tau)$ in the ramp protocol is mixed, so \mathcal{L}_F does not simplify to Eq. (6) in this case. As a result, \mathcal{L}_F must be evaluated using the Uhlmann fidelity [Eq. (3)], which is numerically more demanding and more sensitive to accumulated floating-point noise when \mathcal{L}_F becomes very small [80]. Subsequently, we are able to gather the data of \mathcal{L}_F and corresponding f_F only until $N = 500$, and furthermore, we had to identify numerical zeros using the threshold $\varepsilon = 10^{-13}$, which is two orders of magnitude larger than the machine precision. As in the quench protocol, we define times $t_c^{(1)}$ and $t_c^{(1)}$ as the first times at which \mathcal{L}_F respectively drops below and rises above the numerical zero. The first critical time is then obtained as $t_c^{(1)} = (t_c^{(1)} + t_c^{(1)})/2$ as before. The resulting values are listed in Tab. III. The corresponding rate function $f_F(t)$ is shown in Fig. 5 (b), which exhibits the expected singular behavior at $t_c^{(1)}$.

The finite-size scaling of the first critical time for the ramp protocol is shown in Fig. 6 for the same values of parameters used in Fig. 5. The data support convergence to a constant in the $N \rightarrow \infty$ limit, with a substantially faster approach than in the quench case for

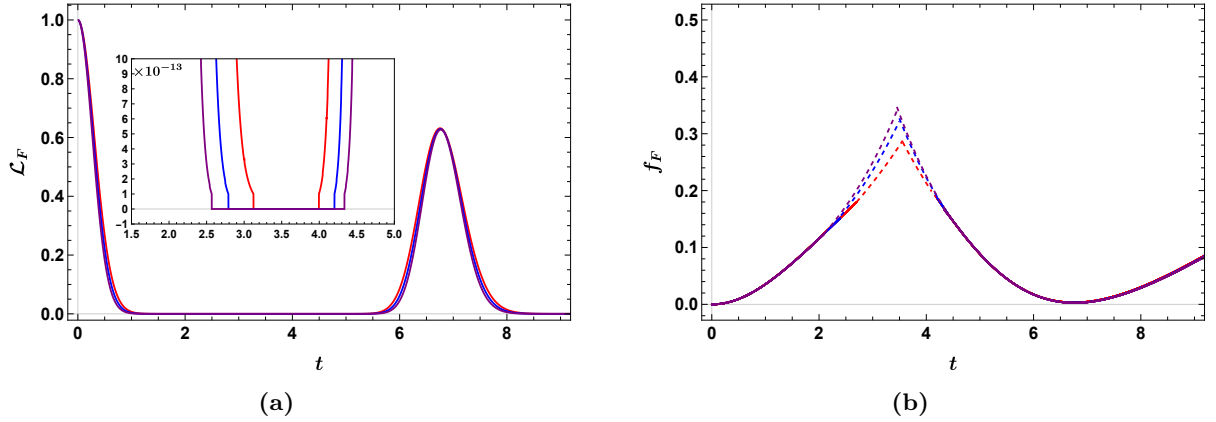


FIG. 5. *DQPT under a finite-time ramp from the non-BTC to the BTC phase.* (a) The fidelity-based Loschmidt echo \mathcal{L}_F is shown during the post-ramp unitary evolution for $N = 70$ (red), $N = 80$ (blue), and $N = 90$ (purple). The parameter ω_0 is ramped linearly from $\omega_{0,i} = 0$ to $\omega_{0,f} = -1$ over a duration $\tau = 5$ according to Eq. (12) under Lindblad dynamics, after which dissipation is switched off and the system evolves unitarily. \mathcal{L}_F is computed with respect to the mixed state at the end of the ramp. The first zero of \mathcal{L}_F defines the critical time $t_c^{(1)}$. The inset magnifies the region near the t -axis. Numerical zeros are identified using a threshold of 10^{-13} . The values of $t_c^{(1)}$ are listed in Tab. III. (b) The rate function f_F corresponding to (a) is shown with the curves of the same colors for the respective N values as in (a). At the first critical time $t_c^{(1)}$, where \mathcal{L}_F vanishes, f_F exhibits a cusp-like singularity, confirming the presence of a DQPT under the ramp protocol. Solid curves are generated for numerically accessible values, while dashed curves show extrapolations inside the numerically inaccessible region.

N	$t_{\downarrow}^{(1)}$	$t_{\uparrow}^{(1)}$	$t_c^{(1)}$
70	3.123	3.995	3.559
80	2.789	4.202	3.496
90	2.567	4.335	3.451

TABLE III. *Ramp protocol: non-BTC \rightarrow BTC.* The values of $t_{\downarrow}^{(1)}$, $t_{\uparrow}^{(1)}$, and $t_c^{(1)}$ in Fig. 5 (a) corresponding to $N = 70$, 80, and 90.

the accessible system sizes. The red dots are the actual data, whereas the blue curve is the best power-law fit of the form $t_c(N) = aN^{-b} + c$ for the full range of data shown in Fig. 6 with best-fit values of fitting parameters as $a = 1.045 \times 10^4 \pm 9.513 \times 10^1$, $b = 2.5$ and $c = 3.319 \pm (< 10^{-3})$. The RMS fitting error is 0.003. Since the time resolution used to generate the time evolution is $\Delta t = 0.001$, we truncate the best-fit parameter values and their errors at the third decimal place. Note that since the amount of data available for fitting is limited to $N \leq 500$ for the reasons described earlier the numerical routine employed for fitting is not able to fit the function $aN^{-b} + c$ with three parameters. To mitigate this, we have varied the parameter b by hand while fitting the other two parameters for each choice of b and found that the RMS error is minimized for $b = 2.5$. In conclusion, we find that in the $N \rightarrow \infty$ limit $t_c^{(1)}$ approaches a value of 3.319 via a power-law with an exponent of 2.5.

V. CONCLUSION

In this work, we have demonstrated that dynamical quantum phase transitions occur in a Markovian open

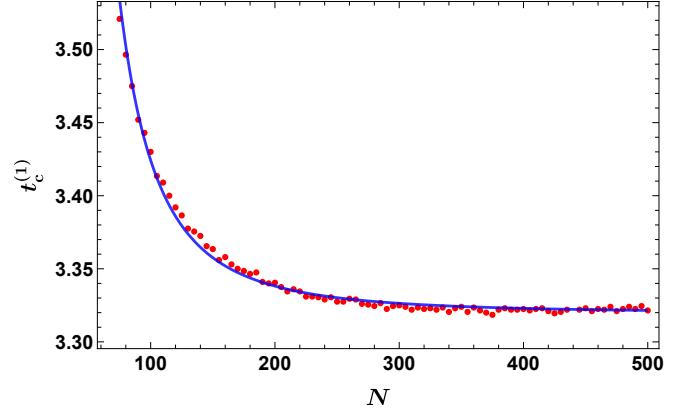


FIG. 6. *Finite-size scaling of the first critical time for the ramp protocol.* The first critical time $t_c^{(1)}$ is plotted as a function of system size N for the non-BTC \rightarrow BTC ramp. The red dots represent the numerical data, while the blue curve is a power-law fit $t_c^{(1)}(N) = aN^{-b} + c$, demonstrating convergence to a constant value in the thermodynamic limit. The best-fit values of fitting parameters are $a = 1.045 \times 10^4 \pm 9.513 \times 10^1$, $b = 2.5$ and $c = 3.319 \pm (< 10^{-3})$. The RMS fitting error is 0.003. The values of all the parameters are the same as in Fig. 5.

quantum many-body system that supports a boundary time-crystal phase. Using the fidelity-based Loschmidt echo suitable for mixed-state Lindblad dynamics, we identified nonanalyticities in the corresponding rate function following both sudden quenches and finite-time ramps across the BTC transition. We extracted the finite-size scaling of the first critical time and showed

convergence toward a well-defined thermodynamic-limit value, with distinct scaling exponents for quench and ramp protocols. When the post-quench parameters lie in the BTC phase, the system approaches a time-periodic steady state, and the Loschmidt echo exhibits repeated zeros, leading to a sequence of DQPT critical times. In contrast, when the dynamics relaxes to a stationary steady state outside the BTC phase, the first critical time can be followed by a regime without revivals. More broadly, our results show that DQPTs extend into

genuinely dissipative time-crystalline phases and are not restricted to closed or Floquet systems.

ACKNOWLEDGMENTS

We acknowledge that the computations were performed using ARMADILLO [81, 82] on the cluster computing facility of the Harish-Chandra Research Institute, India.

[1] Frank Wilczek, “Quantum time crystals,” *Phys. Rev. Lett.* **109**, 160401 (2012).

[2] Patrick Bruno, “Comment on “quantum time crystals”,” *Phys. Rev. Lett.* **110**, 118901 (2013).

[3] Patrick Bruno, “Impossibility of spontaneously rotating time crystals: A no-go theorem,” *Phys. Rev. Lett.* **111**, 070402 (2013).

[4] Haruki Watanabe and Masaki Oshikawa, “Absence of quantum time crystals,” *Phys. Rev. Lett.* **114**, 251603 (2015).

[5] Krzysztof Sacha and Jakub Zakrzewski, “Time crystals: a review,” *Reports on Progress in Physics* **81**, 016401 (2017).

[6] Vedika Khemani, Roderich Moessner, and S. L. Sondhi, “A Brief History of Time Crystals,” (2019), arXiv:1910.10745 [cond-mat.str-el].

[7] Dominic V. Else, Christopher Monroe, Chetan Nayak, and Norman Y. Yao, “Discrete time crystals,” *Annual Review of Condensed Matter Physics* **11**, 467–499 (2020).

[8] Michael P. Zaletel, Mikhail Lukin, Christopher Monroe, Chetan Nayak, Frank Wilczek, and Norman Y. Yao, “Colloquium: Quantum and classical discrete time crystals,” *Rev. Mod. Phys.* **95**, 031001 (2023).

[9] Dominic V. Else, Bela Bauer, and Chetan Nayak, “Floquet time crystals,” *Phys. Rev. Lett.* **117**, 090402 (2016).

[10] J. Zhang *et al.*, “Observation of a discrete time crystal,” *Nature* **543**, 217–220 (2017), arXiv:1609.08684 [quant-ph].

[11] Vedika Khemani, Achilleas Lazarides, Roderich Moessner, and S. L. Sondhi, “Phase structure of driven quantum systems,” *Phys. Rev. Lett.* **116**, 250401 (2016).

[12] C. W. von Keyserlingk, Vedika Khemani, and S. L. Sondhi, “Absolute stability and spatiotemporal long-range order in floquet systems,” *Phys. Rev. B* **94**, 085112 (2016).

[13] Wen Wei Ho, Soonwon Choi, Mikhail D. Lukin, and Dmitry A. Abanin, “Critical Time Crystals in Dipolar Systems,” *Phys. Rev. Lett.* **119**, 010602 (2017), arXiv:1703.04593 [cond-mat.dis-nn].

[14] J. Randall, C. E. Bradley, F. V. van der Gronden, A. Galicia, M. H. Abobeih, M. Markham, D. J. Twitchen, F. Machado, N. Y. Yao, and T. H. Taminiau, “Many-body-localized discrete time crystal with a programmable spin-based quantum simulator,” *Science* **374**, abk0603 (2021), arXiv:2107.00736 [quant-ph].

[15] Dominic V. Else, Bela Bauer, and Chetan Nayak, “Prethermal phases of matter protected by time-translation symmetry,” *Phys. Rev. X* **7**, 011026 (2017).

[16] Tomotaka Kuwahara, Takashi Mori, and Keiji Saito, “Floquet–Magnus theory and generic transient dynamics in periodically driven many-body quantum systems,” *Annals Phys.* **367**, 96–124 (2016), arXiv:1508.05797 [quant-ph].

[17] Dmitry Abanin, Wojciech De Roeck, Wen Wei Ho, and François Huveneers, “A rigorous theory of many-body prethermalization for periodically driven and closed quantum systems,” *Communications in Mathematical Physics* **354**, 809–827 (2017).

[18] Dmitry A. Abanin, Wojciech De Roeck, Wen Wei Ho, and François Huveneers, “Effective hamiltonians, prethermalization, and slow energy absorption in periodically driven many-body systems,” *Phys. Rev. B* **95**, 014112 (2017).

[19] David J. Luitz, Roderich Moessner, S. L. Sondhi, and Vedika Khemani, “Prethermalization without temperature,” *Phys. Rev. X* **10**, 021046 (2020).

[20] F. Iemini, A. Russomanno, J. Keeling, M. Schirò, M. Dalmonte, and R. Fazio, “Boundary time crystals,” *Phys. Rev. Lett.* **121**, 035301 (2018).

[21] Giulia Piccitto, Matteo Wauters, Franco Nori, and Nathan Shammah, “Symmetries and conserved quantities of boundary time crystals in generalized spin models,” *Phys. Rev. B* **104**, 014307 (2021).

[22] Gianluca Passarelli, Procolo Lucignano, Rosario Fazio, and Angelo Russomanno, “Dissipative time crystals with long-range lindbladians,” *Phys. Rev. B* **106**, 224308 (2022).

[23] Luis Fernando dos Prazeres, Leonardo da Silva Souza, and Fernando Iemini, “Boundary time crystals in collective d -level systems,” *Phys. Rev. B* **103**, 184308 (2021).

[24] Federico Carollo and Igor Lesanovsky, “Exact solution of a boundary time-crystal phase transition: time-translation symmetry breaking and non-Markovian dynamics of correlations,” (2021), 10.1103/PhysRevA.105.L040202, arXiv:2110.00030 [cond-mat.stat-mech].

[25] Antônio C. Lourenço, Luis Fernando dos Prazeres, Thiago O. Maciel, Fernando Iemini, and Eduardo I. Duzzioni, “Genuine multipartite correlations in a boundary time crystal,” *Phys. Rev. B* **105**, 134422 (2022), arXiv:2112.11510 [quant-ph].

[26] Álvaro Rubio-García, Ángel L. Corps, Armando Relaño, Rafael A. Molina, Francisco Pérez-Bernal, José Enrique García-Ramos, and Jorge Dukelsky, “Exceptional spectral phase in a dissipative collective spin model,” *Phys. Rev. A* **106**, L010201 (2022), arXiv:2202.09337 [quant-ph].

ph].

[27] Albert Cabot, Leah Sophie Muhle, Federico Carollo, and Igor Lesanovsky, “Quantum trajectories of dissipative time crystals,” *Phys. Rev. A* **108**, L041303 (2023), arXiv:2212.06460 [quant-ph].

[28] Victor Montenegro, Marco G. Genoni, Abolfazl Bayat, and Matteo G. A. Paris, “Quantum metrology with boundary time crystals,” *Commun. Phys.* **6**, 304 (2023), arXiv:2301.02103 [quant-ph].

[29] Federico Carollo, Igor Lesanovsky, Mauro Antezza, and Gabriele De Chiara, “Quantum thermodynamics of boundary time-crystals,” *Quantum Sci. Technol.* **9**, 035024 (2024), arXiv:2306.07330 [quant-ph].

[30] Albert Cabot, Federico Carollo, and Igor Lesanovsky, “Continuous Sensing and Parameter Estimation with the Boundary Time Crystal,” *Phys. Rev. Lett.* **132**, 050801 (2024), arXiv:2307.13277 [quant-ph].

[31] Dominic Gribben, Anna Sanpera, Rosario Fazio, Jamir Marino, and Fernando Iemini, “Boundary Time Crystals as AC sensors: enhancements and constraints,” *SciPost Phys.* **18**, 100 (2025), arXiv:2406.06273 [quant-ph].

[32] Paulo J. Paulino, Albert Cabot, Gabriele De Chiara, Mauro Antezza, Igor Lesanovsky, and Federico Carollo, “Thermodynamics of coupled time crystals with an application to energy storage,” *Quantum Sci. Technol.* **11**, 015003 (2026), arXiv:2411.04836 [quant-ph].

[33] Gianluca Passarelli, Angelo Russomanno, and Procolo Lucignano, “Nonstabilizerness of a boundary time crystal,” *Phys. Rev. A* **111**, 062417 (2025), arXiv:2503.05243 [quant-ph].

[34] Zhuqing Wang, Ruochen Gao, Xiaoling Wu, Berislav Buća, Klaus Mølmer, Li You, and Fan Yang, “Boundary Time Crystals Induced by Local Dissipation and Long-Range Interactions,” *Phys. Rev. Lett.* **135**, 230401 (2025), arXiv:2503.20761 [quant-ph].

[35] Albert Cabot, Federico Carollo, and Igor Lesanovsky, “Quantum enhanced parameter estimation with monitored quantum nonequilibrium systems using inefficient photo detection,” (2025), arXiv:2503.21753 [quant-ph].

[36] Dominik Nemeth, Alessandro Principi, and Ahsan Nazir, “Solving boundary time crystals via the superspin method,” (2025), arXiv:2507.06998 [quant-ph].

[37] Bandita Das, Rahul Ghosh, and Victor Mukherjee, “Stabilizing boundary time crystals through Non-markovian dynamics,” (2025), arXiv:2508.09688 [quant-ph].

[38] Eoin O’Connor, Victor Montenegro, Francesco Albarelli, Matteo G. A. Paris, Abolfazl Bayat, and Marco G. Genoni, “Attaining Quantum Sensing Enhancement from Monitored Dissipative Time Crystals,” (2025), arXiv:2508.15448 [quant-ph].

[39] Zeping Liu, Yaotian Li, Zhaoyu Fei, and Xiaoguang Wang, “Boundary Time Crystals: Beyond Mean-Field Theory,” (2025), arXiv:2510.03028 [quant-ph].

[40] Malik Jirasek, Igor Lesanovsky, and Albert Cabot, “The Boundary Time Crystal as a light source for quantum enhanced sensing beyond the Heisenberg Limit,” (2025), arXiv:2511.23416 [quant-ph].

[41] M. Heyl, A. Polkovnikov, and S. Kehrein, “Dynamical quantum phase transitions in the transverse-field ising model,” *Phys. Rev. Lett.* **110**, 135704 (2013).

[42] Markus Heyl, “Dynamical quantum phase transitions: a review,” *Rept. Prog. Phys.* **81**, 054001 (2018), arXiv:1709.07461 [cond-mat.stat-mech].

[43] Subir Sachdev, *Quantum Phase Transitions* (Cambridge University Press, 2011).

[44] S. L. Sondhi, S. M. Girvin, J. P. Carini, and D. Shashar, “Continuous quantum phase transitions,” *Rev. Mod. Phys.* **69**, 315–333 (1997).

[45] Nick Fläschner, Dominik Vogel, Matthias Tarnowski, Benno S. Rem, Dirk-Sören Lühmann, Markus Heyl, Jan Carl Budich, Ludwig Mathey, Klaus Sengstock, and Christof Weitenberg, “Observation of dynamical vortices after quenches in a system with topology,” *Nature Phys.* **14**, 265–268 (2017), arXiv:1608.05616 [cond-mat.quant-gas].

[46] J. Zhang, G. Pagano, P. W. Hess, A. Kyprianidis, P. Becker, H. Kaplan, A. V. Gorshkov, Z. X. Gong, and C. Monroe, “Observation of a many-body dynamical phase transition with a 53-qubit quantum simulator,” *Nature* **551**, 601–604 (2017), arXiv:1708.01044 [quant-ph].

[47] P. Jurcevic, H. Shen, P. Hauke, C. Maier, T. Brydges, C. Hempel, B. P. Lanyon, M. Heyl, R. Blatt, and C. F. Roos, “Direct observation of dynamical quantum phase transitions in an interacting many-body system,” *Phys. Rev. Lett.* **119**, 080501 (2017).

[48] Tian Tian, Yongguan Ke, Liang Zhang, Shaochun Lin, Zhifu Shi, Pu Huang, Chaohong Lee, and Jiangfeng Du, “Observation of dynamical phase transitions in a topological nanomechanical system,” *Phys. Rev. B* **100**, 024310 (2019).

[49] Xue-Yi Guo, Chao Yang, Yu Zeng, Yi Peng, He-Kang Li, Hui Deng, Yi-Rong Jin, Shu Chen, Dongning Zheng, and Heng Fan, “Observation of a dynamical quantum phase transition by a superconducting qubit simulation,” *Phys. Rev. Appl.* **11**, 044080 (2019).

[50] Kunkun Wang, Xingze Qiu, Lei Xiao, Xiang Zhan, Zhi-hao Bian, Wei Yi, and Peng Xue, “Simulating dynamic quantum phase transitions in photonic quantum walks,” *Phys. Rev. Lett.* **122**, 020501 (2019).

[51] H.-X. Yang, T. Tian, Y.-B. Yang, L.-Y. Qiu, H.-Y. Liang, A.-J. Chu, C. B. Dağ, Y. Xu, Y. Liu, and L.-M. Duan, “Observation of dynamical quantum phase transitions in a spinor condensate,” *Phys. Rev. A* **100**, 013622 (2019).

[52] T. Tian, H.-X. Yang, L.-Y. Qiu, H.-Y. Liang, Y.-B. Yang, Y. Xu, and L.-M. Duan, “Observation of dynamical quantum phase transitions with correspondence in an excited state phase diagram,” *Phys. Rev. Lett.* **124**, 043001 (2020).

[53] Xinfang Nie, Bo-Bo Wei, Xi Chen, Ze Zhang, Xiuzhu Zhao, Chudan Qiu, Yu Tian, Yunlan Ji, Tao Xin, Dawei Lu, and Jun Li, “Experimental observation of equilibrium and dynamical quantum phase transitions via out-of-time-ordered correlators,” *Phys. Rev. Lett.* **124**, 250601 (2020).

[54] James Dborin, Vinul Wimalaweera, Fergus Barratt, Eric Ostby, Thomas E. O’Brien, and Andrew G. Green, “Simulating groundstate and dynamical quantum phase transitions on a superconducting quantum computer,” *Nature Commun.* **13**, 5977 (2022), arXiv:2205.12996 [quant-ph].

[55] Simon Karch *et al.*, “Probing quantum many-body dynamics using subsystem Loschmidt echos,” (2025), arXiv:2501.16995 [cond-mat.quant-gas].

[56] A. A. Zvyagin, “Dynamical quantum phase transitions,” (2017), arXiv:1701.08851 [cond-mat.stat-mech].

[57] Markus Heyl, “Dynamical quantum phase transitions: a brief survey,” *EPL* **125**, 26001 (2019), [arXiv:1811.02575 \[cond-mat.stat-mech\]](https://arxiv.org/abs/1811.02575).

[58] Souvik Bandyopadhyay, Sudarshana Laha, Utso Bhattacharya, and Amit Dutta, “Exploring the possibilities of dynamical quantum phase transitions in the presence of a Markovian bath,” *Sci. Rep.* **8**, 11921 (2018), [arXiv:1804.03865 \[cond-mat.stat-mech\]](https://arxiv.org/abs/1804.03865).

[59] Haifeng Lang, Yixin Chen, Qiantan Hong, and Heng Fan, “Dynamical quantum phase transition for mixed states in open systems,” *Phys. Rev. B* **98**, 134310 (2018).

[60] Thi Ha Kyaw, Victor M. Bastidas, Jirawat Tangpanitanon, Guillermo Romero, and Leong-Chuan Kwek, “Dynamical quantum phase transitions and non-markovian dynamics,” *Phys. Rev. A* **101**, 012111 (2020).

[61] S. Morrison and A. S. Parkins, “Dynamical quantum phase transitions in the dissipative lipkin-meshkov-glick model with proposed realization in optical cavity qed,” *Phys. Rev. Lett.* **100**, 040403 (2008).

[62] Valentin Link and Walter T. Strunz, “Dynamical phase transitions in dissipative quantum dynamics with quantum optical realization,” *Phys. Rev. Lett.* **125**, 143602 (2020).

[63] J. Naji, Masoud Jafari, R. Jafari, and Alireza Akbari, “Dissipative floquet dynamical quantum phase transition,” *Phys. Rev. A* **105**, 022220 (2022).

[64] Grazia Di Bello, Andrea Ponticelli, Fabrizio Pavan, Vittorio Cataudella, Giulio De Filippis, Antonio de Candia, and Carmine Antonio Perroni, “Environment induced dynamical quantum phase transitions in two-qubit Rabi model,” *Commun. Phys.* **7**, 364 (2024), [arXiv:2312.05697 \[quant-ph\]](https://arxiv.org/abs/2312.05697).

[65] Kohei Kawabata, Anish Kulkarni, Jiachen Li, Tokiro Numasawa, and Shinsei Ryu, “Dynamical quantum phase transitions in sachdev-ye-kitaev lindbladians,” *Phys. Rev. B* **108**, 075110 (2023).

[66] N. Sedlmayr, M. Fleischhauer, and J. Sirker, “Fate of dynamical phase transitions at finite temperatures and in open systems,” *Phys. Rev. B* **97**, 045147 (2018).

[67] Kai Zhang, Chang Shu, and Kai Sun, “Dynamical Quantum Phase Transitions and Many-Body Backflow in Open Quantum Systems,” (2025), [arXiv:2509.03570 \[quant-ph\]](https://arxiv.org/abs/2509.03570).

[68] Gilles Perez and Vincenzo Alba, “Smearing of dynamical quantum phase transitions in dissipative free-fermion systems,” (2025), [arXiv:2509.21585 \[cond-mat.stat-mech\]](https://arxiv.org/abs/2509.21585).

[69] Arkadiusz Kosior and Krzysztof Sacha, “Dynamical quantum phase transitions in discrete time crystals,” *Phys. Rev. A* **97**, 053621 (2018).

[70] Julia Hannukainen and Jonas Larson, “Dissipation-driven quantum phase transitions and symmetry breaking,” *Phys. Rev. A* **98**, 042113 (2018).

[71] D. F. Walls, P. D. Drummond, S. S. Hassan, and H. J. Carmichael, “Non-equilibrium phase transitions in cooperative atomic systems,” *Progress of Theoretical Physics Supplement* **64**, 307–320 (1978), <https://academic.oup.com/ptps/article-pdf/doi/10.1143/PTPS.64.307/5292058/64-307.pdf>.

[72] P.D. Drummond and H.J. Carmichael, “Volterra cycles and the cooperative fluorescence critical point,” *Optics Communications* **27**, 160–164 (1978).

[73] R.R. Puri and S.V. Lawande, “Exact steady-state density operator for a collective atomic system in an external field,” *Physics Letters A* **72**, 200–202 (1979).

[74] D F Walls, “Cooperative fluorescence from n coherently driven two-level atoms,” *Journal of Physics B: Atomic and Molecular Physics* **13**, 2001 (1980).

[75] S. Schneider and G. J. Milburn, “Entanglement in the steady state of a collective-angular-momentum (dicke) model,” *Phys. Rev. A* **65**, 042107 (2002).

[76] Tatjana Puskarov and Dirk Schuricht, “Time evolution during and after finite-time quantum quenches in the transverse-field Ising chain,” *SciPost Phys.* **1**, 003 (2016).

[77] Shraddha Sharma, Uma Divakaran, Anatoli Polkovnikov, and Amit Dutta, “Slow quenches in a quantum ising chain: Dynamical phase transitions and topology,” *Phys. Rev. B* **93**, 144306 (2016).

[78] A. Uhlmann, “The “transition probability” in the state space of a_* -algebra,” *Reports on Mathematical Physics* **9**, 273–279 (1976).

[79] Richard Jozsa, “Fidelity for Mixed Quantum States,” *J. Mod. Opt.* **41**, 2315–2323 (1994).

[80] Note that Eq. (9) involves products of large density matrices for larger N values whereas Eq. (6) computes just a single matrix element. The consequence of this is that the computation of Eq. (9) is prone to faster accumulation of numerical noise during the time evolution compared to Eq. (6). This accumulation of noise during the time evolution is very prominent when the value of \mathcal{L}_F becomes very small which happens precisely near its zeros.

[81] Conrad Sanderson and Ryan Curtin, “Armadillo: a template-based c++ library for linear algebra,” *Journal of Open Source Software* **1**, 26 (2016).

[82] Conrad Sanderson and Ryan Curtin, “A user-friendly hybrid sparse matrix class in c++,” in *Mathematical Software – ICMS 2018* (Springer International Publishing, 2018) p. 422–430.